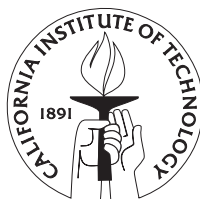


CHAMBER STUDIES OF SECONDARY ORGANIC AEROSOL FORMATION

Thesis by
Nga Lee Ng

In Partial Fulfillment of the Requirements for the
Degree of Doctor of Philosophy



California Institute of Technology

Pasadena, California

2007

(Defended May 22, 2007)

© 2007

Nga Lee Ng

All Rights Reserved

學貴有恆

“Perseverance is the key to learning.” – Chinese proverb

Acknowledgements

Looking back at my years at Caltech, I feel blessed every step along the way. It has been such a wonderful journey, not just because of all the great science in the roof lab, but also the many wonderful people that I got to know and become friends with.

I would like to express my sincere gratitude to my advisors, Professor John Seinfeld and Professor Richard Flagan, for their continuous trust, support, and guidance throughout the years. Their scientific insights are invaluable, and their enthusiasm about science is especially inspiring. I thank them for giving me the opportunity to join the lab. Despite their busy schedules, John and Rick are always there when I need guidance. They have been truly supportive and understanding and I could not ask for better advisors. I would also like to thank my thesis committee members, Professor Paul Wennberg and Professor Michael Hoffmann, for their valuable time and comments. I also thank my undergrad advisor, Professor Chak Chan, for introducing me to the field of atmospheric science and for his constant support.

I have been very fortunate to be part of such a supportive, friendly, and fun research group. I would like to thank the past and present group members, especially the lab people for making every day in the lab so enjoyable: Tomtor Varutbangkul, Roya Bahreini, Melita Keywood, Tracey Rissman, Song Gao, Jesse Kroll, Jason Surratt, Shane Murphy, Armin Sorooshian, Harmony Gates, Arthur Chan, and Puneet Chhabra. Because of the collaborative nature of our work, I could not have got all the work done without their help. They are also a constant source of laughter and encouragement; with them even the most stressful periods in the lab seem more manageable. I also thank the

“modelers” of the group, Philip Stier, Daven Henze, Anne Chen, Candy Tong, Amir Hakami, and Julia Lu for their support.

I am especially grateful to Tomtor and Roya for their patience in teaching me so many things in the lab, from little things like “the difference between a back ferrule and a front ferrule”, to how to operate the many instruments, and for always being there to help me even when they were overwhelmed with their own work. The two and a half years with Jesse in the lab have been incredible. We built our friendship through running hundreds and hundreds of chamber experiments (final checks!), and together we survived the ups and downs of the experiments. Jesse taught me so much about atmospheric chemistry and I am grateful for his patience and guidance. I considered myself extraordinarily lucky to have the opportunity to work so closely with such a great scientist and I treasure our friendship dearly.

I am grateful to Nathan Dalleska for his help with GC troubleshooting, Richard Gerhart for fixing/making the numerous glasswares for us, to Mike Vondrus for his help in machining various parts of the experimental setup. I would also like to thank Ann Hilgenfeldt and Yvette Grant for placing endless orders for repairs and parts. A big thanks also goes to Kathy Bubash for her administrative help.

I am glad to have met so many wonderful friends outside the lab who made my time here enjoyable, especially Joyce Poon, Michelle Friedman, Marcelo Guzman, Peter Leong, Shahin Rahman, Tonci Crmaric, Nikoo Saber, Mike Rubel, Anita Lee, as well as my “Hong Kong friends” at Caltech. I enjoyed all the fun activities we had. Fourth year is an especially fun-filled year for me, because of some very special friends, Tracey Rissman, Adam Olsen, Philip Stier, and Marco Seidel. I will always remember all the

happy times we shared. I would also like to thank Jang Wook Choi, whether we were working on problem sets or studying for quals, I really appreciate his companionship and support.

Even though I am thousands of miles away from home, my friends on the other side of the ocean keep showering me with their support and encouragement throughout the years and I am very grateful for that. A very special thanks goes to Yee Man Lai, for being such a great friend for almost twenty years and for always sharing my dreams with me.

Finally, I thank my parents, my sister, and my brother for their love and support. I am grateful to my parents for instilling within me the importance of learning and to never to give up, for their unwavering trust in my abilities, and for understanding my move far away from home to follow my own path. I could not have finished this without the unceasing support and encouragement they have given me throughout my life.

Abstract

Atmospheric oxidation of volatile organic compounds leads to the formation of secondary organic aerosol (SOA). Laboratory chambers provide a controlled environment for investigating aerosol formation and evolution. This thesis presents results on aerosol formation from a wide range of parent organic compounds under a variety of experimental conditions.

The effect of particle-phase acidity on aerosol formation is explored in a series of alkene ozonolysis experiments. Oligomeric species are detected regardless of the particle-phase acidity, indicating the ubiquitous existence of particle-phase reactions. As acidity increases, larger oligomers are formed more abundantly and aerosol yields also increase. Volatile organic compounds generally not considered to be SOA precursors, including isoprene and glyoxal, have been shown to lead to aerosol formation. Uptake of glyoxal into particles is evidence that small molecules can potentially produce aerosol via reactive absorption. Although there is strong evidence that heterogeneous reactions play an important role in SOA formation, the detailed mechanisms remain poorly understood. In a comprehensive study on aerosol formation from biogenic hydrocarbons, it is found that data on aerosol growth as a function of the amount of hydrocarbon reacted provide important insights into the general aerosol formation mechanisms by identifying rate-determining steps and whether SOA is formed from first- or second-generation products.

The mechanism of aerosol formation by isoprene is specifically investigated over a range of NO_x concentrations. Aerosol yields are found to decrease substantially with increasing NO_x . The same NO_x dependence is observed for monoterpenes (α -pinene), as well as aromatic hydrocarbons (*m*-xylene, toluene, and benzene). It is suggested that

peroxy radical chemistry plays the central role in the observed NO_x dependence. The NO_x dependence for larger compounds is, however, different from that of isoprene, monoterpenes, and aromatics. For sesquiterpenes such as longifolene and aromadendrene, aerosol yields increase with increasing NO_x concentration. The reversal of the NO_x dependence of SOA formation for the sesquiterpenes appears to be the result of formation of relatively nonvolatile organic nitrates, and/or the isomerization of large alkoxy radicals that leads to less volatile products.

Table of Contents

Acknowledgements.....	iv
Abstract.....	vii
List of Tables	xv
List of Figures.....	xvii
Chapter 1: Introduction.....	1
Chapter 2: Contribution of First- versus Second-Generation Products to Secondary Organic Aerosols Formed in the Oxidation of Biogenic Hydrocarbons.....	5
2.1 Abstract.....	6
2.2 Introduction.....	7
2.3 Experimental.....	11
2.4 Results.....	15
2.4.1 Ozonolysis studies	15
2.4.2 Photooxidation studies.....	16
2.5 Discussion.....	17
2.5.1 Time-dependent vs. final SOA growth	19
2.5.1.1 α -pinene ozonolysis (one double bond).....	19
2.5.1.2 Terpinolene ozonolysis (more than one double bond).....	20
2.5.2 Chemistry of individual compounds.....	22
2.5.2.1 α -pinene ozonolysis.....	22
2.5.2.2 α -pinene photooxidation.....	23
2.5.2.3 Terpinolene ozonolysis	24
2.5.2.4 Terpinolene and limonene photooxidation	26

2.5.2.5 Isoprene photooxidation.....	27
2.5.2.6 Other compounds with multiple double bonds	28
2.5.2.7 β -caryophyllene ozonolysis	29
2.5.2.8 Longifolene photooxidation.....	30
2.6 Implications for aerosol formation.....	31
2.7 Acknowledgements.....	33
2.8 References.....	34
Chapter 3: Particle Phase Acidity and Oligomer Formation in Secondary Organic Aerosol	70
3.1 Abstract.....	71
3.2 Introduction.....	71
3.3 Experimental.....	73
3.4 Results and discussion	75
3.5 Acknowledgements.....	80
3.6 References.....	80
Chapter 4: Chamber Studies of Secondary Organic Aerosol Growth by Reactive Uptake of Simple Carbonyls	90
4.1 Abstract.....	91
4.2 Introduction.....	91
4.3 Experimental.....	97
4.4 Results and discussion	103
4.4.1 Uptake of organics: carbonyl compounds other than glyoxal	103
4.4.2 Uptake of organics: glyoxal.....	105

4.5 Implications.....	109
4.6 Acknowledgements.....	115
4.7 References.....	115
Chapter 5: Secondary Organic Aerosol Formation from Isoprene Photooxidation under High-NO _x Conditions.....	131
5.1 Abstract.....	132
5.2 Introduction.....	132
5.3 Experimental.....	135
5.4 Results and discussion	136
5.5 Acknowledgements.....	141
5.6 References.....	141
Chapter 6: Secondary Organic Aerosol Formation from Isoprene Photooxidation.....	148
6.1 Abstract.....	149
6.2 Introduction.....	149
6.3 Experimental.....	153
6.4 Results.....	155
6.4.1 Blank Runs.....	155
6.4.2 Low-NO _x experiments	155
6.4.3 High-NO _x experiments.....	157
6.4.4 Isoprene oxidation products.....	159
6.5 Discussion.....	159
6.5.1 General mechanism of aerosol growth	159
6.5.2 Role of NO _x	162

6.5.3 Rapid photochemical loss of SOA.....	166
6.6 Acknowledgements.....	168
6.7 References.....	168
Chapter 7: Effect of NO _x on Secondary Organic Aerosol (SOA) Formation from Photooxidation of Terpenes	188
7.1 Abstract.....	189
7.2 Introduction.....	189
7.3 Experimental Section.....	191
7.4 Aerosol Yields	196
7.4.1 α -pinene photooxidation.....	196
7.4.2 Longifolene photooxidation.....	197
7.4.3 Aromadendrene photooxidation.....	198
7.5 Chemical composition of SOA	199
7.5.1 Aerosol Mass Spectrometer (Q-AMS) measurements.....	199
7.5.2 Offline chemical analysis.....	201
7.6 Discussion.....	203
7.6.1 Effect of hydrocarbon size on NO _x dependence	203
7.6.2 General mechanisms of aerosol growth.....	207
7.6.2.1 Loss of semivolatiles.....	207
7.6.2.2 SOA formation from higher generation products	209
7.7 Implications.....	210
7.8 Appendix: Description of PTR-MS technique.....	212
7.9 Acknowledgements.....	214

7.10 References.....	214
Chapter 8: Secondary Organic Aerosol Formation from <i>m</i> -xylene, toluene, and benzene	241
8.1 Abstract.....	242
8.2 Introduction.....	242
8.3 Experimental.....	245
8.4 Results.....	248
8.4.1 High-NO _x conditions	248
8.4.2 Low-NO _x conditions	251
8.4.3 SOA yield parameters	252
8.5 Discussion.....	254
8.5.1 Effect of NO _x on SOA yields.....	254
8.5.2 Effect of oxidation rate	257
8.5.3 General mechanism of SOA formation.....	260
8.5.4 Effect of seed acidity	262
8.6 Implication for SOA growth from aromatic hydrocarbons.....	263
8.7 Acknowledgements.....	264
8.8 References.....	265
Chapter 9: Conclusions.....	290
Appendix A: Reactions of Semivolatile Organics and Their Effects on Secondary Organic Aerosol Formation	295
Appendix B: Low-Molecular-Weight and Oligomeric Components in Secondary Organic Aerosol from the Ozonolysis of Cycloalkenes and α -Pinene.....	302

Appendix C: Chemical Composition of Secondary Organic Aerosol Formed from the Photooxidation of Isoprene	321
Appendix D: Evidence for Organosulfates in Secondary Organic Aerosol	348
Appendix E: Characterization of 2-Methylglyceric Acid Oligomers in Secondary Organic Aerosol Formed from the Photooxidation of Isoprene Using Trimethylsilylation and Gas Chromatography/Ion Trap Mass Spectrometry	360
Appendix F: Measurements of Secondary Organic Aerosol from Oxidation of Cycloalkenes, Terpenes, and <i>m</i> -xylene Using an Aerodyne Aerosol Mass Spectrometer	377
Appendix G: Secondary Aerosol Formation from Atmospheric Reactions of Aliphatic Amines	393
Appendix H: Hygroscopicity of Secondary Organic Aerosols Formed by Oxidation of Cycloalkenes, Monoterpenes, Sesquiterpenes, and Related Compounds.....	419
Appendix I: Gas-Phase Products and Secondary Aerosol Yields from the Ozonolysis of Ten Different Terpenes	442
Appendix J: Gas-Phase Products and Secondary Aerosol Yields from the Photooxidation of 16 Different Terpenes.....	461

List of Tables

Table 2. 1. Parent hydrocarbon studied	43
Table 2. 2. Initial conditions and data for ozonolysis experiments	46
Table 2. 3. Initial conditions and data for photooxidation experiments	47
Table 2. 4. Ozonolysis - major first-generation products and their molar yields	48
Table 2. 5. Photooxidation - major first-generation products and their molar yields	49
Table 4. 1. Experimental conditions and measured particle growth for glyoxal uptake experiments ^A	126
Table 5. 1. Experimental conditions and results	145
Table 6. 1. Experimental conditions and results for NO _x -free experiments. ¹	177
Table 6. 2. Experimental conditions and results for high-NO _x experiments. ¹	178
Table 7. 1. Parent hydrocarbons studied	220
Table 7. 2. Initial conditions and data for α -pinene experiments	221
Table 7. 3. Initial conditions and data for longifolene experiments	222
Table 7. 4. Initial conditions and data for aromadendrene experiments	223
Table 7. 5. Estimated effective SOA densities	224
Table 7. 6. α -Pinene acidic SOA components detected by the UPLC/ESI-TOFMS instrument	225
Table 7. 7. Longifolene SOA components detected by the UPLC/ESI-TOFMS instrument	226
Table 8. 1. Aromatic hydrocarbons studied	272
Table 8. 2. Initial conditions and data for high-NO _x (HONO) experiments	273
Table 8. 3. Initial conditions and data for low-NO _x (H ₂ O ₂) experiments	274

Table 8. 4. Initial conditions and data for acid/nonacid experiments	275
Table 8. 5. Estimated effective SOA densities	276
Table 8. 6. Aerosol yield parameters	277

List of Figures

Figure 2. 1. α -pinene ozonolysis and aerosol mass formation	50
Figure 2. 2. Terpinolene ozonolysis and aerosol mass formation.....	51
Figure 2. 3. Time-dependent growth curves for all compounds studied in ozonolysis experiments (except linalool, which does not have significant aerosol growth), note that the axes have different scales.....	52
Figure 2. 4. Time-dependent growth curves for all compounds studied in photooxidation experiments (except longifolene, which is shown in Figure 2.20), note that the axes have different scales.....	53
Figure 2. 5. Time-dependent and final growth curves for α -pinene ozonolysis. The large diamonds represent final growth data through which the yield curve has been fit.....	54
Figure 2. 6. AMS relative delta time series plot for α -pinene ozonolysis. Unsaturated organics yield delta values ≤ 0 , and oxygenated organics yield delta values ≥ 2	55
Figure 2. 7. Time-dependent and final growth curves for terpinolene ozonolysis. The large diamonds represent final growth data through which the yield curve has been fit.	56
Figure 2. 8. Time evolution of pinonaldehyde in α -pinene ozonolysis. The concentration of pinonaldehyde is the average of the upper and lower limits measured by PTR-MS (20).	57

Figure 2. 9. Time evolution of pinonaldehyde in α -pinene photooxidation. The concentration of pinonaldehyde is the mid-range mixing ratio measured by PTR-MS (21).	58
Figure 2. 10. Time evolution of m/z 93 and m/z 111 ions for terpinolene ozonolysis; m/z 93 is the dehydrated fragment of m/z 111.	59
Figure 2. 11. The amount of the intermediate product m/z 111 (including the dehydrated fragment m/z 93) measured, formed and reacted over time for terpinolene ozonolysis	60
Figure 2. 12. SOA mass formed as a function of the amount of the intermediate product m/z 111 reacted for terpinolene ozonolysis	61
Figure 2. 13. SOA mass formed as a function of the amount of the intermediate product m/z 111 reacted for terpinolene photooxidation	62
Figure 2. 14. SOA mass formed as a function of the amount of the intermediate product m/z 169 (including its fragments and isotopes) reacted for limonene photooxidation	63
Figure 2. 15. Time evolution of methacrolein + methyl vinyl ketone for isoprene photooxidation	64
Figure 2. 16. SOA mass formed as a function of the amount of the methacrolein + methyl vinyl ketone reacted for isoprene photooxidation	65
Figure 2. 17. β -caryophyllene ozonolysis and aerosol mass formation	66
Figure 2. 18. β -caryophyllene and ozone reacted over the course of the experiment (Table 2.2: Experiment on 3/21/2003)	67

Figure 2. 19. AMS relative delta time series plot for β -caryophyllene ozonolysis.

Unsaturated organics yield delta values ≤ 0 , and oxygenated organics yield delta values ≥ 2 68

Figure 2. 20. Growth curve for longifolene photooxidation..... 69

Figure 3. 1. The relative yield difference (RYD) of SOA between the acid and nonacid

cases for seven pairs of α -pinene ozonolysis experiments on MgSO_4 seeds, two pairs on $(\text{NH}_4)_2\text{SO}_4$ seeds, as well as two pairs of terpinolene ozonolysis experiments on MgSO_4 seeds. The absolute SOA yield is defined as the mass of SOA produced relative to the mass of hydrocarbon consumed. The RYD is defined as the difference in the absolute SOA yield between the acid and nonacid cases normalized to the nonacid-case yield. Corresponding to the seven α -pinene mixing ratios shown (i.e., 12ppb, 25ppb, 48ppb, 52ppb, 96ppb, 120ppb and 135ppb), the absolute SOA yields are 0.30, 0.32, 0.35, 0.38, 0.46, 0.52 and 0.53, respectively, for the nonacid cases, and are 0.41, 0.43, 0.44, 0.47, 0.53, 0.57, 0.57, respectively, for the acid cases..... 82

Figure 3. 2. Ion trap mass spectrum (+ ion mode) of the extract of SOA from the

ozonolysis of (a) 120 ppb α -pinene on MgSO_4 -only seed (RH = 55%). In the m/z range up to 1600, the average background ion intensity is ~ 400000 , which is labeled as the dashed line in this and the following MS, unless noted otherwise. See Supporting Information, Figure 3.S3, for a typical background MS. (b) 120 ppb α -pinene on MgSO_4 - H_2SO_4 seed. Other experimental conditions are identical to (a). (c) 72 ppb α -pinene on $(\text{NH}_4)_2\text{SO}_4$ -only seed.

Other experimental conditions are identical to (a). (d) 72 ppb α -pinene on $(\text{NH}_4)_2\text{SO}_4$ - H_2SO_4 seed. Other experimental conditions are identical to (a).. 83

- Figure 3. 3. MS/MS (- ion mode) of (a) 357 ion in the SOA from the same α -pinene ozonolysis experiment as in Figure 3.2(a), its likely structure and fragmentation (hydrogen rearrangement and dehydrogenation not shown), and the structure of the monomer. See Supporting Information, Figure 3.S5 for the detailed structures of fragment ions. (b) 245 ion in the SOA from 1-methyl cyclopentene ozonolysis, its likely structures and fragmentation, and the structures of the monomers..... 86
- Figure 3. 4. Ion trap mass spectrum (+ ion mode) of the extract of SOA from the ozonolysis of 180ppb α -pinene in the presence of dry $(\text{NH}_4)_2\text{SO}_4$ -only seed. Large amounts of both small and large oligomers are present in this SOA. .. 88
- Figure 3. 5. Ion trap mass spectrum (+ ion mode) of the extract of SOA from the ozonolysis of 50ppb α -pinene in the absence of seed particles. This IT-MS is similar to that of the SOA from its parallel ozonolysis experiment in the presence of MgSO_4 seed particles, and is also similar to that of the SOA from other α -pinene ozonolysis experiments, such as the one shown in Figure 3.2(a). The background ion intensities are lower than 5% of the maximum intensity ($m/z = 381.0$, designated as 100%)...... 89
- Table 4. 1. Experimental conditions and measured particle growth for glyoxal uptake experiments^A..... 126
- Figure 4. 1. Structures of the carbonyls studied in this work. 127

- Figure 4. 2. Sample DMA volume data for chamber experiments. Introduction of inorganic seed corresponds to $t=0$; the gradual decrease in volume is a result of particle loss to the chamber walls. Grey circles: inorganic seed only. Black circles: inorganic seed (ammonium sulfate/sulfuric acid), followed by introduction of 500 ppb 2,4-hexadienal at $t=50$ min (dashed line). Data are scaled so that starting particle volumes are equivalent. 128
- Figure 4. 3. DMA volume data growth for a glyoxal + inorganic seed experiment. As in Figure 4.2, introduction of inorganic seed corresponds to $t=0$. Grey circles: inorganic seed only. Black circles: inorganic seed (ammonium sulfate/sulfuric acid), followed by introduction of 200 ppb glyoxal at $t=53$ min (dashed line). Data are scaled so that starting particle volumes are equivalent. 129
- Figure 4. 4. Particle growth as a function of gas-phase glyoxal concentration and initial seed volume, assuming unit density of the organic fraction of the aerosol. Black circles: ammonium sulfate seed. Grey squares: mixed ammonium sulfate/sulfuric acid seed. The fit shown is to the ammonium sulfate data only. The dashed line near the bottom of the figure is the growth expected using the measured Henry's Law constant (in seawater) of 3.6×10^5 M/atm [Zhou and Mopper, 1990]. 130
- Figure 5. 1. A typical experiment (no. 6 in Table 5.1), showing [isoprene] (black circles), $[O_3]$ (dark gray lines), $[NO]$ (light gray lines), $[NO_2]$ (black lines), and particle volume increase (black dots) as a function of reaction time. Gaps in the O_3 and NO_x data are a result of switching between chambers. 146
- Figure 5. 2. Aerosol growth as a function of concentration of isoprene reacted. 147

Figure 6. 1. Structures and measured yields of first-generation products of the OH-initiated oxidation of isoprene under high-NO _x conditions. ^a Tuazon and Atkinson (5). ^b Paulson et al. (6). ^c Miyoshi et al. (7). ^d Sprengnether et al. (8). ^e Chen et al. (9). ^f Zhao et al. (10). ^g Baker et al. (11).....	179
Figure 6. 2. Reaction profile of a typical isoprene photooxidation experiment under NO _x -free conditions (Experiment 5).	180
Figure 6. 3. Typical AMS spectrum (m/z ≥ 40) of SOA formed from isoprene photooxidation under low-NO _x conditions. For clarity, masses in which the organics overlap with peaks from sulfate (m/z 48-50, 64-66, 80-83, 98-100) and tungsten (from the filament; m/z 182, 184-186) have been omitted. Light gray bars correspond to negative values after data analysis.	181
Figure 6. 4. Measured SOA growth versus isoprene reacted (low-NO _x conditions). Gray circles: maximum growth; black circles: final growth, after photochemical loss of SOA (see text for details). Each pair of points (at a single value of isoprene reacted) corresponds to one experiment. Data are taken from Table 6.1; SOA mass is calculated using a density of 1.25 g/cm ³	182
Figure 6. 5. Reaction profile of a typical isoprene photooxidation experiment under high-NO _x conditions (Experiment 11). Decay of isoprene is rapid, with most consumed in the first 30 minutes of reaction, so is omitted for clarity.....	183
Figure 6. 6. Typical AMS spectrum of SOA formed from isoprene photooxidation under high-NO _x conditions. See description of Figure 6.3 for details.	184

Figure 6. 7. SOA growth as a function of initial NO _x concentration, for a fixed isoprene concentration (45 ± 4 ppb). Results shown are from Table 6.2; the NO _x -free point is final growth from Experiment 2, Table 6.1.	185
Figure 6. 8. AMS spectrum of SOA formed from methacrolein photooxidation under high-NO _x conditions. See description of Figure 6.3 for details. The spectrum shown is similar to that of isoprene photooxidation (Figure 6.6), with the same major peaks, suggesting the importance of methacrolein as an intermediate in SOA formation from isoprene oxidation under high-NO _x conditions.	186
Figure 6. 9. Reaction mechanism of isoprene oxidation, showing the formation of first-generation products. For clarity, only one of four possible alkyl radicals and one of six possible hydroperoxy radicals are shown. The first-generation reaction products are all unsaturated so may be rapidly oxidized to second-generation products.	187
Figure 7. 1. Time-dependent growth curves for α-pinene photooxidation under different NO _x conditions.	227
Figure 7. 2. Time-dependent growth curves for longifolene photooxidation under high- and low-NO _x conditions. The mixing ratios in the legend refer to the amount of longifolene reacted in each experiment.	228
Figure 7. 3. Time-dependent growth curves for longifolene photooxidation with H ₂ O ₂ as an OH precursor. Aerosol growth in the presence of ~300 ppb NO (Experiment 7 in Table 7.3) exceeds that without NO.	229
Figure 7. 4. SOA growth as a function of initial NO _x concentrations, for a fixed longifolene concentration (~4.3 ppb). Results shown are from Table 7.3.	230

- Figure 7. 5. SOA growth as a function of initial NO_x concentration, at a fixed initial aromadendrene concentration (~5 ppb). Results shown are from Table 7.4. 231
- Figure 7. 6. AMS high-NO_x spectra signal versus low-NO_x spectra signal for α-pinene photooxidation. Each mass fragment is normalized by the total signal. The solid black line is the one-to-one line. The spectra are taken when all hydrocarbon has been consumed. 232
- Figure 7. 7. AMS high-NO_x spectra signal versus low-NO_x spectra signal for longifolene photooxidation. Each mass fragment is normalized by the total signal. The solid black line is the 1:1 line. The spectra are taken when all hydrocarbon has been consumed..... 233
- Figure 7. 8. Ratio of the sum of masses at *m/z* 30 and 46 to total organic mass as a function of organic mass as measured by the AMS for α-pinene photooxidation. The higher ratio for high- NO_x experiments suggests the formation of nitrate species..... 234
- Figure 7. 9. Ratio of the sum of masses at *m/z* 30 and 46 to total organic mass as a function of organic mass as measured by the AMS for longifolene photooxidation. The higher ratio for high- NO_x experiments suggests the formation of nitrate species..... 235
- Figure 7. 10. Changes in AMS spectrum over the course of longifolene photooxidation under high-NO_x conditions. Top panel: Fractional contribution of each mass fragment to the total organic and nitrate signal during the growth phase of the experiment. Bottom panel: Percentage change of each mass fragment from the growth phase to the point at which all of the hydrocarbon is consumed..... 236

Figure 7. 11. Changes in AMS spectrum over the course of longifolene photooxidation under low-NO_x conditions. Top panel: Fractional contribution of each mass fragment to the total organic and nitrate signal during the growth phase of the experiment. Bottom panel: Percentage change of each mass fragment from the growth phase to the point at which all of the hydrocarbon is consumed..... 237

Figure 7. 12. UPLC/ESI-TOFMS extracted ion chromatograms (EICs) ($= m/z$ 346 + 374 + 390) for longifolene photooxidation experiments. The even $[M - H]^-$ ion s listed above the chromatographic peaks correspond to organic nitrates detected in longifolene SOA. No organic nitrates are detected in the H₂O₂ experiment. The HONO experiment has the widest array of organic nitrates detected (as shown in Table 7.7), as well as the largest chromatographic peaks; m/z 372 is the only exception, and is most abundant in the “H₂O₂ + NO” experiment. These EICs are directly comparable as the volume of chamber air sampled is approximately the same (2 m³). 238

Figure 7. 13. General schematic of gas-phase peroxy radical chemistry in SOA formation. 239

Figure 7. 14. A kinetic scheme depicting the competition between gas-particle partitioning and irreversible loss of the gas-phase semivolatiles. X represents the product of generic loss of semivolatile species A_g by chemical reaction, and/or loss to chamber walls. k' is the pseudo-first-order rate constant ($k' = k_{OH}[OH]$) for photooxidation of the parent hydrocarbon; k_g is the first-order rate constant of loss of semivolatiles..... 240

Figure 8. 1. Typical reaction profile of a high-NO _x experiment in which HONO is used as the OH precursor (initial conditions: 89.3 ppb of <i>m</i> -xylene, 470 ppb NO, and 473 ppb NO ₂).	278
Figure 8. 2 (a). Reaction profile of a typical classical photooxidation experiment (initial conditions: 101.6 ppb <i>m</i> -xylene, 97 ppb NO, and 26 ppb NO ₂). (b) Reaction profile of a classical photooxidation experiment in the presence of ~1 ppm NO _x (initial conditions: 94.8 ppb <i>m</i> -xylene, 878 ppb NO, and 65 ppb NO ₂). A negligible amount of ozone is formed during the experiment, and no SOA is formed.	279
Figure 8. 3. Time-dependent growth curves for <i>m</i> -xylene photooxidation under high-NO _x conditions. The concentrations in the legend refer to the amount of <i>m</i> -xylene reacted in each experiment.	281
Figure 8. 4. Time-dependent growth curves for toluene photooxidation under high-NO _x conditions. The concentrations in the legend refer to the amount of toluene reacted in each experiment.	282
Figure 8. 5. Time-dependent growth curves for benzene photooxidation under high- and low-NO _x conditions. Under high-NO _x conditions, the initial benzene concentration is 337 ppb (12% reacted). Under low-NO _x conditions, the initial benzene concentration is 395 ppb (16% reacted) and the system has a constant yield of 37%.	283
Figure 8. 6. Time-dependent growth curves for <i>m</i> -xylene photooxidation under low-NO _x conditions. The concentrations in the legend refer to the amount of <i>m</i> -xylene reacted in each experiment. The system exhibits a constant yield of 36%...	284

- Figure 8. 7. Time-dependent growth curves for toluene photooxidation under low-NO_x conditions. The concentrations in the legend refer to the amount of toluene reacted in each experiment. The system exhibits a constant yield of 30%... 285
- Figure 8. 8. Yield curves for toluene and *m*-xylene under high-NO_x conditions. The parameters for fitting the yield curves are, toluene: $\alpha_1 = 0.058$, $K_{om,1} = 0.430$, $\alpha_2 = 0.113$, and $K_{om,2} = 0.047$; *m*-xylene: $\alpha_1 = 0.031$, $K_{om,1} = 0.761$, $\alpha_2 = 0.090$, and $K_{om,2} = 0.029$ 286
- Figure 8. 9. Time-dependent growth curves for toluene photooxidation in the presence of neutral seed versus acidic seed. 287
- Figure 8. 10. A simplified SOA formation mechanism for toluene photooxidation. X represents the generic non particle-phase product from all gas-phase loss processes. 288
- Figure 8. 11. Comparison of *m*-xylene high-NO_x yield curve obtained in the current work to that from Odum et al. (1996). The yield curve from Odum et al. (1996) has been corrected for the temperature (25°C) of this study and density (1.48 g cm⁻³) of the SOA..... 289

Chapter 1

Introduction

Introduction

Aerosols are suspended solid or liquid particles and they affect air quality, human health and the earth's climate. Aerosols can be classified into two main categories according to their formation processes. Primary aerosols are emitted directly from different sources into the atmosphere, while the oxidation of organic gases leads to the formation of low-volatility products that partition into the condensed phase and result in the formation of secondary organic aerosol (SOA). Biogenic hydrocarbons emitted by vegetation and aromatics from anthropogenic sources are important precursors for SOA formation. The main oxidants in the atmosphere are ozone (O_3), hydroxyl radical (OH), and nitrate radical (NO_3). SOA contributes significantly to the total ambient organic aerosols in urban areas, as well as regionally and globally.

Laboratory chambers provide a controlled environment to study the formation and evolution of secondary organic aerosol, by isolating specific compounds of interest and controlling the oxidation environment. Since identification and quantification of all oxidation products from parent hydrocarbons are difficult, aerosol yields have been used in the study of secondary precursor organics. Aerosol yields indicate the aerosol-forming potential of various precursor organics. Yield is defined as the ratio of the mass concentration of aerosol formed from the oxidation of a given parent hydrocarbon to that of the hydrocarbon reacted: $Y = \Delta M_o / \Delta HC$, where ΔM_o ($\mu g m^{-3}$) is the organic aerosol mass produced for a certain reacted amount of hydrocarbon ΔHC ($\mu g m^{-3}$). While yield curves (Y plotted against ΔM_o) have proven to be useful in representing SOA formation, the general mechanisms of SOA formation cannot be readily inferred. In chapter 2 it is shown that this model can be extended for interpretation of laboratory SOA growth data

in terms of underlying chemistry, by plotting experimentally measured aerosol growth, ΔM_o , as a function of the amount of hydrocarbon reacted, ΔHC (growth curve). The growth curve approach is applied in a comprehensive study on aerosol formation from biogenic hydrocarbons to study the general aerosol formation mechanisms.

In chapter 3 the effect of particle-phase acidity on aerosol formation is explored in a series of alkene ozonolysis experiments, including α -pinene and 6 cycloalkenes of various carbon numbers and substitutions. The aerosol yields from α -pinene ozonolysis are systematically studied over a range of initial hydrocarbon concentrations, in the presence of seed particles of differing acidity. The composition of the aerosols formed are presented.

Volatile organic compounds previously not considered to be SOA precursors, including glyoxal and isoprene, are shown to lead to aerosol formation. In chapter 4 the potential for aerosol growth via heterogeneous reactions for a number of small carbonyls is examined by measuring changes in particle volume and composition when inorganic seed and gas-phase carbonyls are introduced into the chambers. Glyoxal is the only single carbonyl that leads to substantial aerosol growth and this reactive uptake is discussed in detail. Chapter 5 presents the results on the first study on secondary organic aerosol formation from isoprene photooxidation under high- NO_x conditions in which HONO is used as the OH precursor. In chapter 6 the mechanism of aerosol formation by isoprene photooxidation is comprehensively investigated over a range of experimental conditions, namely isoprene and NO_x concentrations. The effect of NO_x concentration on aerosol yields and composition is discussed. In chapter 7 the effect of NO_x levels on SOA formation from photooxidation of larger biogenic hydrocarbons such as monoterpenes

(α -pinene) and sesquiterpenes (longifolene and aromadendrene) are investigated by performing experiments under two limiting NO_x conditions, as well as varying the amount of NO_x present systematically. The SOA yields and composition under different NO_x conditions is presented.

Besides biogenic compounds, aerosol formation from aromatic hydrocarbons, including *m*-xylene, toluene, and benzene are investigated under different NO_x conditions. The results are presented in chapter 8. Additionally, the effect of seed aerosol acidity on SOA formation is studied under both high- and low-NO_x conditions. The SOA yield parameters obtained at the two NO_x limits allow one to parameterize the NO_x dependence of SOA formation for use in atmospheric models.

Finally, chapter 9 summarizes the findings presented in the previous seven chapters. Appendix A presents results from a kinetic model of the behavior of a semivolatile compound which may undergo irreversible reactions in both the gas and particle phases in addition to partitioning. The effect of such loss processes on aerosol yields is discussed. Appendices B-J present results on studies of SOA composition and formation mechanisms with a wide range of instruments and analytical techniques, including filter sample analysis (Appendices B-E), Aerosol Mass Spectrometer (AMS, Appendices F and G), and Hygroscopicity Tandem Differential Mobility Analyzer (HTDMA, Appendix H). The gas-phase composition from the ozonolysis and photooxidation of various biogenic hydrocarbons are studied in detail with a Proton Transfer Reaction Mass Spectrometer (PTR-MS) and the results are presented in Appendices I and J.